ChemElectroChem

Research Article
doi.org/10.1002/celc.202400457

Chemistry Europe
European Chemical Societies Publishing

www.chemelectrochem.org

Electrocatalytic Performance and Kinetic Behavior of Anion-Intercalated Borate-Based NiFe LDH in Alkaline OER

Maike Berger,[a] Alexandra Markus,[a] Stefan Palkovits,[a] and Regina Palkovits*[a, b]

The synthesis of hydrogen *via* water electrolysis is an important step towards resolving the energy crisis and impeding global warming, as hydrogen can be used as a green energy carrier. The oxygen evolution as one half-cell reaction (OER) is currently limiting efficient water splitting due to kinetic inhibition as well as a complex mechanism, causing a large overpotential. Nickel-iron layered double hydroxides (LDH) were found to be suitable OER catalysts, as they are cost effective, stable and highly active. This work focuses on the intercalation of different organic and inorganic borates into the LDH interlayers to study their influence on OER. Besides activity and stability measurements, three borate candidates were chosen for a kinetic study, including steady-state Tafel analysis and reaction order plots. It was found that the Bockris pathway with the second step as rate-determining step was predominant for all three catalysts. Of all candidates, the intercalation of borate resulted in the highest performance, which was associated with a high reducibility affecting the active metal sites.

Introduction

The development of effective and low-cost catalysts for water electrolysis is oblige for green hydrogen to be a viable alternative to conventional energy sources, since it can be used for energy storage of renewable energies.[1] The mayor issue here is the large overpotential due to kinetic inhibition which hinders efficient energy conversion. Of both half-cell reactions, oxygen formation at the anode holds a greater impact on the overall required potential caused by a complex electron transfer mechanism.[2,3] Possible reaction pathways for OER in alkaline media are listed in Table 1.[4] To lower the OER overpotential, suitable catalysts that relieve electron transfer and optimize oxygen formation are obligatory to make water electrolysis efficient and competitive. Many efforts have been made over the past decades in terms of synthesizing, characterizing and tuning catalysts to achieve highly active and long-term stable systems.[5] Noble-metal based electrocatalysts such as RuO_2 or IrO_2 have shown the best performance, but their scarcity and high cost make these catalysts not suitable for economic hydrogen production.[3,6]

As alternative to noble-metal based catalysts, 3d transition metals were identified, which are cost-efficient, earth abundant and provide catalytic activity and durability under alkaline conditions. According to Bockris and Otagawa,[9] Trasatti[10] and Rossmeisl *et al.*[11] the good activity of transition-metal based catalysts in OER was attributed to the 3delectron number of the metal ions, the enthalpy of a lower to higher oxide transition and the surface oxygen binding.[12] Nevertheless, it is still difficult to date to predict transition metal catalysts with high OER activity by means of these proposed descriptors. Our group made a contribution to increase this generalizability of descriptive characters in electrocatalytic systems.[13–15] Mürtz *et al.* studied OER on perovskite $LaCo_{1-x}B_xO_3$ (B = Al, Ni, Zn) and found that covalency in the interaction of O 2p transition metal 3d states, e_g occupancy and the charge transfer energy (CTE) are linear descriptors for the electrocatalytic performance, regarding overpotential, Tafel slope and charge transfer resistance.[13] It was concluded that the catalysts' covalency and CTE show a negative, whereas e_g occupancy shows a positive correlation with OER activity. We also presented in our group how forecasts for water oxidation catalysts can be made based

Table 1. Possible mechanisms for the oxygen evolution reaction in alkaline media.[4]

Electrochemical oxide path[7]	Oxide path[7]
$M + OH^- \rightarrow MOH + e^-$ $MOH + OH^- \rightarrow MO + H_2O + e^-$ $2\,MO \rightarrow O_2 + 2\,M$	$M + OH^- \rightarrow MOH + e^-$ $2\,MOH \rightarrow MO + M + H_2O$ $2\,MO \rightarrow 2\,M + O_2$
Krasil'shchikov path[8]	O'Grady's path[4]
$M + OH^- \rightarrow MOH + e^-$ $MOH + OH^- \rightarrow MO^- + H_2O$ $MO^- \rightarrow MO + e^-$ $2\,MO \rightarrow 2\,M + O_2$	$M + OH^- \rightarrow MOH + e^-$ $M^zOH \rightarrow M^{z+1}OH + e^-$ $2\,M^{z+1}OH + 2\,OH^- \rightarrow 2\,H_2O + O_2$
Bockris' Path[9]	
$M + OH^- \rightarrow MOH + e^-$ $MOH + OH^- \rightarrow MH_2O_2 + e^-$ $MH_2O_2 + OH^- \rightarrow MHO_2^- + H_2O$ $MH_2O_2 + MHO_2^- \rightarrow O_2 + H_2O + OH^- + 2\,M$	

[a] *M. Berger, A. Markus, S. Palkovits, Prof. R. Palkovits*
Institute of Technical and Macromolecular Chemistry, RWTH Aachen University, Aachen 52074, Germany
E-mail: palkovits@itmc.rwth-aachen.de
Homepage: https://www.itmc.rwth-aachen.de/

[b] *Prof. R. Palkovits*
Institute for Sustainable Hydrogen Economy (INW-2), Forschungszentrum Jülich, Marie-Curie-Str. 5, Jülich 52428, Germany

Supporting information for this article is available on the WWW under https://doi.org/10.1002/celc.202400457

on machine learning approaches.[14] Therefore, about 6000 published samples of (Ni–Fe–Co–Ce)O_x catalysts with known composition and OP (at 10 mA cm^{-2}) were used to train different machine learning algorithms. We could show that already simple models like artificial neural networks were able to give a decent prediction quality and were capable to outperform more complicated models. Another contributor to OER kinetics was found to be the spin state transition from H_2O/OH^- to O_2.[16] Li *et al.* studied the spin state density of Ni-MOF by introducing transition metals into the framework.[17] They found that OER activity has a volcanic relationship with the d-band center, where NiFe-MOF was at the volcano summit, benefiting from the synergistic effect of electronegativity sites and high-density spin state, which balances the adsorption/desorption of intermediates, and minimizes the energy barrier for OER.

Among the transition-metal based catalysts for OER catalysis, layered double hydroxides have gained great interest in recent years. Trotochaud *et al.* studied oxygen evolution on thin transition metal oxide films and found that $Ni_{0.9}Fe_{0.1}O_x$ was the most active water oxidation catalyst, with roughly one order of magnitude higher activity than IrO_x films. The high activity was attributed to the *in situ* formation of layered NiFeOOH species with nearly every Ni atom being electrochemically active.[18] In addition to their great catalytic activity, their flexible structural composition and the broad range of available synthesis methods make LDHs one of the most advanced electrocatalysts towards alkaline water splitting.[3,19] They possess a layered and open structure, whereas the hydroxyl groups pointing into the interlayer region favor the formation of hydrogen bonds to interlayer anions and water molecules.[20,21] Due to the relatively weak interlayer bonding, LDH materials exhibit interlayer expanding properties, which opens up the possibility to introduce foreign anions and organic molecules.[20] Luo *et al.* successfully intercalated NiFe LDH with phosphorus oxoanions *via* a simple co-precipitation process.[22] The anions strongly interacted with the edge-sharing MO_6 layers, resulting in a modification of the surface electronic structure of the Ni sites. NiFe LDH intercalated with $H_2PO_2^-$ delivered superior OER performance with a low onset overpotential of 215 mV and a Tafel slope of only 38 mV dec^{-1}.[23] Zhou *et al.* systematically investigated the effect of redox-active interlayer anions by intercalating 16 anions with different reducing abilities.[24] They showed that intercalated anions with strong reducing ability modify the electronic structure of surface-metal sites and can significantly improve the performance of NiFe LDH. While these studies mainly focus on achieving superior catalysis performances, little effort has been made to gain a deeper understanding of why these performance differences based on intercalation of different anions occur. In fact, few studies aimed for a mechanistical view on alkaline OER over such Nickel based catalysts.[5,25,26] Scarr *et al.* for example conducted a study of oxygen evolution on nickel and other metals and found that for nickel and its alloys, a dual Tafel behavior appeared.[8] Based on these findings, they proposed a mechanism which suggests that following the electrochemical adsorption of an hydroxide ion, the formation of an adsorbed hydrogen peroxide radical ion, $MO_2H_2^-$, occurs which is then discharged and dehydrogenated to oxygen. The stated, so called adsorbed hydrogen peroxide mechanism for alkaline OER, was also validated in other studies.[27] In view of these findings, our working group investigated the kinetic behavior of NiFe LDH with three different intercalated anions (CO_3^{2-}, $H_2PO_2^-$ and $B(OH)_4^-$) which also showed a dual Tafel behavior for all candidates.[25] We observed fractional reaction orders which were validated together with the Tafel slopes by Temkin adsorption conditions. While the Bockris' mechanism was valid for all candidates, the change in Tafel slope could be attributed to a change in rate determining step (RDS). Understanding the influence of material properties on the mechanism in OER is of fundamental relevance to enable a knowledge-based catalyst design, and identifying kinetic bottlenecks allows for a better control and process design.[5,26]

Herein, different borate-based intercalated NiFe LDHs are prepared by a simple co-precipitation process. Besides borate, tetraborate as well as three different organic borates (named as PBA, BDBA and BPBA) were chosen under otherwise constant synthetic conditions to explore the influence of borates on the catalytic behavior in alkaline OER. For all catalysts, cyclic voltammetry and X-ray diffraction as well as other material analyticswere used to characterize the electro- and physicochemical material properties. For three candidates, steady-state Tafel plots and reaction order measurements were performed to conduct a deeper mechanistic study. Here, steady-state operations refine the determination of Tafel slopes and open up the possibility to select the proper mechanism and adsorption model for calculating the RDS. To further verify the stability of the intercalated NiFe LDHs, chronoamperometry was conducted for one inorganic and one organic borate-intercalated catalyst.

Results and Discussion

NiFe LDH in a ratio of 2:1 with intercalated anionic forms of boric acid (BA), sodium tetraborate (TB), phenylboronic acid (PBA), benzene-1,4-diboronic acid (BDBA) and 4-biphenylboronic acid (BPBA) were prepared *via* a simple co-precipitation process based on the work of Luo *et al.*[22]

The general structure of layered double hydroxides with intercalated charge-balancing anions, as well as the anions used here are shown in Figure 1.

Prior to electrochemical analysis, the existence of boron in all catalysts and similar Fe/Ni ratios of 0.5 (Table S2) were successfully confirmed *via* elemental analysis. X-ray diffraction (XRD) was measured twice, each in the range of $2\theta = 10–90°$ (Figure 2a) and 9–40° (Figure 2b) to investigate their crystal structure and interlamellar spacing. All catalysts show multiple characteristic reflections of NiFe LDH of which the most prominent ones are shown at $2\theta = 12°$ (003), 24° (006), 39° (012) and 60° (110).[28] The intercalated anions are likely not organized enough to result in a reflex and do not have a large scattering power, meaning that all reflexes are originating from nickel and iron in the host layers. For NiFe(BA) LDH and NiFe(TB) LDH the

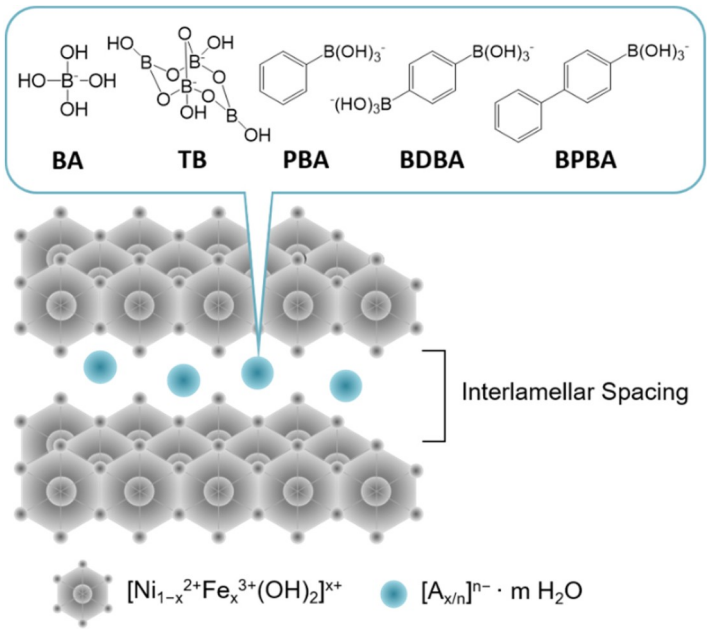

Figure 1. General structure of NiFe LDH with the respective intercalated inorganic (BA and TB) and organic (PBA, BDBA and BPBA) borates.

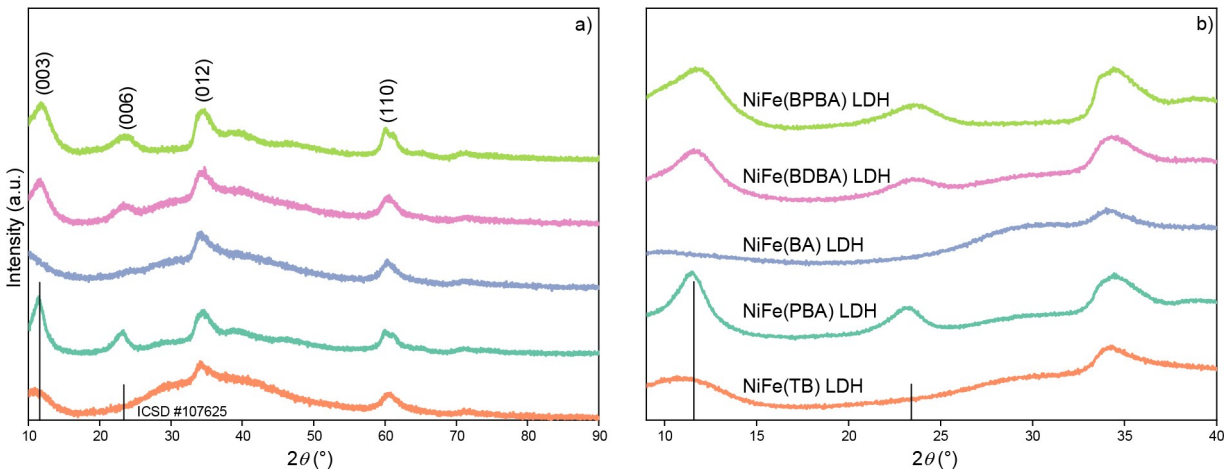

Figure 2. XRD patterns of NiFe LDH containing the anions TB (orange), PBA (turquoise), BA (blue), BDBA (pink) and BPBA (green). The values were collected under CuK_α radiation (λ = 1.54 Å) with 2θ ranging from a) 10° to 90° and b) 9° to 40° in 0.02° steps. Reference lines (black) of the characteristic (003) and (006) Peaks for NiFe(CO_3^{2-}) LDH (ICSD #107625) are marked.

(006) reflex could not be detected. As the (003) and (012) reflections of these catalysts are broad and the (006) reflection shows the least intensity in the other catalysts, it is likely that the (006) reflections are too small to be detected.

A good indication for the success of anion intercalation is the varying basal spacing due to the different molecule sizes of the borates. This spacing can be calculated with the 2θ values of the (003) reflex.[20,29] By using Bragg's law, it follows that the more the reflection is shifted to lower values, the bigger the basal spacing is. The (003) reflections of the aromatic borate intercalated LDH materials all have similar positions with 2θ = 11.50°, 11.62° and 11.74° for NiFe(PBA), (BDBA) and (BPBA) LDH, respectively, resulting in basal spacings of 7.69 Å, 7.61 Å and 7.53 Å. Therefore, the size of anions seems not to have an influence on the basal spacing, which could be explained by the flat alignment of the aromatic molecules, forming stacked layers in the basal space. Aisawa *et al.* studied the intercalation of amino acids in LDH interlayers and found that for aromatic phenylalanine, the LDH basal spacing was smaller than the diameter of the anion. They postulated that the anion is horizontally orientated in the basal spacing, which supports our thesis of a flat alignment of aromats in the interlayer.[30]

Another important information from XRD analysis is the relative intensity of the (003) and (006) reflexes, which is a measure of the interlamellar electron density and thus holds particular importance when intercalating aromatic anions.[31] The higher intensity of the (006) reflection for all organic borates indicate a higher interlamellar electron density com-

pared to (BA) and (TB), suggesting the successful intercalation of the organic borates PBA, BDBA and BPBA. The results for NiFe(TB) LDH and NiFe(BA) LDH must be discussed in more detail. For NiFe(TB) LDH, the (003) reflection appears at $2\theta = 10.82^{\circ}$ resulting in a d-spacing of 8.17 Å whereas NiFe(BA) LDH shows no (003) and (006) reflection, which arises the question about the type of intercalated anion. Under the given synthesis conditions, where the borate species were dissolved in water at pH 10, giving a borate concentration of 0.5 M, boric acid and sodium tetraborate form so called polyborates. According to Anderson *et al.*, dissolving 0.4 M boric acid in water at pH 10 leads to the formation of ~57% $B(OH)_4^-$ and ~23% $B_4O_5(OH)_4^{2-}$ and small amounts of other polynuclear boron species.[32] Therefore it can be assumed that mainly $B(OH)_4^-$ is intercalated into the interlamellar spacing in NiFe(BA) LDH. The lack of (003) and (006) signal and overall low signal intensity can probably be attributed to a small crystallite size or stacking faults.[33]

Although sodium tetraborate was dissolved in the same manner as boric acid, the 4 times higher boron content favors the formation and intercalation of $B_4O_5(OH)_4^{2-}$ (tetraborate anion) into NiFe LDH,[34] resulting in the increased basal spacing of 8.17 Å.

After the successful intercalation of the anions was demonstrated by XRD, electrochemical performance tests were conducted. For OER activity analysis, linear sweep voltammetry was performed in 1 M KOH solution in a classical three-electrode setup. Ni sheet was used as the working electrode, where the catalyst to be analyzed was drop coated on the sheets surface. The LSV curves were recorded at a scan rate of 5 mV s^{-1} and are 100% *iR* corrected to compensate for the electrolyte resistance R_s. The dashed line in Figure 3a marks the potentials to be considered at the defined current density of 100 mA cm^{-2}. As shown in Figure 3b, the overpotentials at 100 mA cm^{-2} (η_{100}) of the candidates follow the order NiFe(BA) < (PBA) < (BDBA) < (BPBA) < (TB) LDH with the respective values of 308 mV, 326 mV, 331 mV, 337 mV and 349 mV. NiFe(BA) LDH shows the highest activity and steepest slope, indicating high reaction rates, followed by NiFe LDH with phenyl borate (PBA) intercalated. The intercalation of tetraborate into the layers led to the worst performance and lowest gradient, indicating slower reaction rates.

Different explanations about how intercalated anions influence the performance of LDHs were made in literature.[22,33,35] Carrasco *et al.* found that increasing the basal spacing to a certain extend through space consuming anions led to lower Tafel slopes and higher activities. Although intercalation of the tetraborate anion in this research increased the basal spacing, this material possessed the lowest performance. This contradiction suggests that other effects have a greater impact on the performance here. Another value to validate different performances of anion intercalated systems is the p*K*a value of the conjugated acid of the anion.[22,33,35] According to Luo *et al.*, a strong reducing agent or Lewis base can induce a lower valence state in the surface nickel atoms. These high-electron nickel sites would then be easier to oxidize, which would improve the OER performance and lower the overpotential.[22] Boric acid is a Lewis acid with the highest p*K*a value of 9.0–9.2 and therefore the strongest Lewis base, which fits to the stated correlation. The other anions have a lower p*K*a, which correlates to a weaker Lewis basicity and thus a lesser interaction with the active sites.[36]

NiFe(PBA) shows a similar, but slightly later onset compared to NiFe(BA) LDH and a gentler slope afterwards, indicating similar activation energy but slower reaction rates. A possible explanation would be that the phenyl group of PBA leads to a greater dislocation of the negative charge in the anion, which could hinder the electrostatic interaction. It is possible that the higher dislocation of the negative charge, due to more possible distinct resonance structures, weakens the Lewis basicity, decreasing the electrostatic interaction and leading to the higher overpotential. NiFe(BDBA) LDH shows a distinct later onset as the previously discussed catalysts. It is possible that a higher dislocation of the negative charge due to more possible distinct resonance structures weakens the Lewis basicity, which

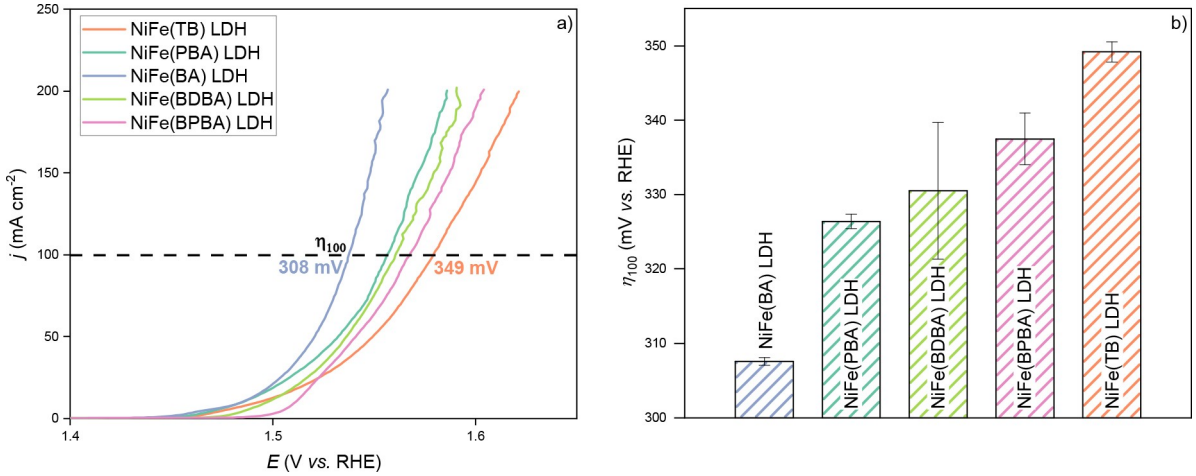

Figure 3. a) Polarization curves of NiFe LDH intercalated with TB (orange), PBA (turquoise), BA (blue), BDBA (green) and BPBA (pink) vs. RHE for the OER. The data points were received at a scan rate of 5 mV s^{-1} using a three-electrode setup with glassy carbon as the counter electrode and Hg/HgO as the reference in 1 M KOH as electrolyte. All curves are 100% iR corrected. b) Comparison of the overpotentials at 100 mA cm^{-2} calculated from the activity curves. All values are 100% iR corrected.

in turn decreases the electrostatic interaction and leads to the higher overpotential. The slope is comparable to NiFe(PBA) LDH, indicating similar kinetics and reaction rates. NiFe(BPBA) shows a late, but harsh onset. The reaction rate of this catalyst is slower but comparable to the reaction rate of (PBA) and (BDBA). The additional phenyl group has an insignificant effect on the kinetics, but a distinct influence on the onset and thus the activation energy.

In addition, the strength and matter of the metal-anion interaction can also influence the reaction rate.[22,23] NiFe(TB) LDH is least active in OER with the highest overpotential of 349 mV. This could be caused by a weaker interaction with the nickel sites, or a slower ion transport, caused by the three dimensionally voluminous nature of tetraborate.

Figure 4 shows Nyquist plots as a result of electrochemical impedance spectroscopy (EIS). Thereby, the diameter of the semicircle is equal to the charge transfer resistance R_{ct}, which describes the electron transfer from the electrode to the liquid and models the overall rate of the OER.[37] Our activity trend is in line with the R_{ct} values of all catalysts. NiFe(BA) LDH obtained the lowest charge transfer resistance, emphasizing its superior catalytic performance. All R_{ct} values are summarized in the SI.

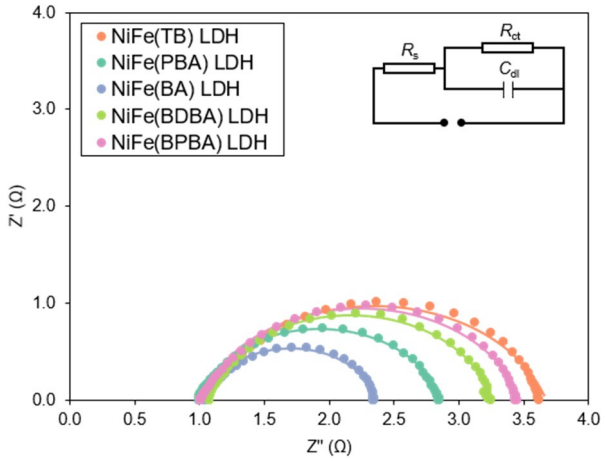

Figure 4. Nyquist plots of all candidates at 0.5 V (vs Hg/HgO) in a frequency range from 100 kHz to 100 mHz at the amplitude of 10 mV. The semicircles were fitted according to the Randles equivalent circuit.

For a more profound insight, a kinetic study was performed for NiFe(BA) as the best performer and two organic candidates, NiFe(PBA) LDH and NiFe(BPBA) LDH. For this purpose, steady-state Tafel plots were conducted around the onset potential from steady-state LSV measurements with 100% *iR* correction (Figure 5a). For all candidates, a change in Tafel slope at around 250 mV overpotential occurred, which can be associated with the onset of OER. In the low Tafel region a slope of 28.7 mV dec^{-1}, 25.5 mV dec^{-1} and 20.6 mV dec^{-1} was obtained for NiFe(PBA), NiFe(BA) and NiFe(BPBA) LDH respectively, whereas 114 mV dec^{-1}, 104 mV dec^{-1}and 131 mV dec^{-1} were obtained in the high region. While the slopes are similar in the low Tafel region (capacitive region), the trend in the high Tafel region fits the activity trend. To determine the rate determining step of the reaction, the transfer coefficient α was further analyzed, in the second Tafel region for all three catalysts. The transfer coefficient can be calculated with Equation (1).

$$\alpha = \frac{1}{b}\left(\frac{2.303\ RT}{F}\right) = \frac{n_f}{v} + n_r\beta \quad (1)$$

Here, b is the Tafel slope, which is inversely proportional to α, meaning that a small slope correlates to a high activity and vice versa.[39] The second part of the equation allows for more mechanistical insight. Hereby, n_f refers to the number of electrons exchanged by the electrode before the RDS, v is the number of occurrences of the RDS in the assumed mechanism, n_r is the number of electrons involved in the RDS and β presents a symmetry factor.[25]

In our previous work, the same assumptions were made about the RDS as in the following (see SI). The elementary steps

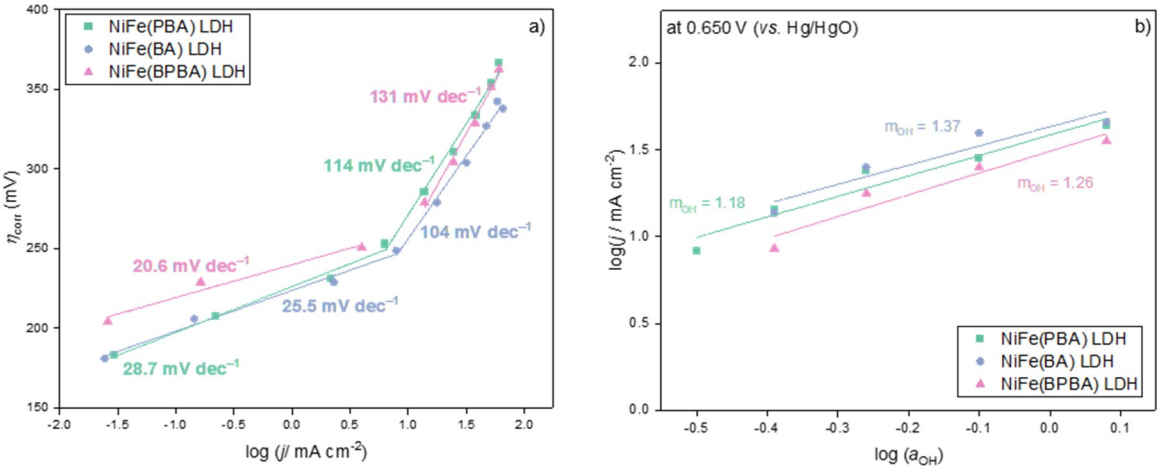

Figure 5. a) Steady-state generated Tafel plots of NiFe LDH with the intercalated anions PBA (green), BA (blue) and BPBA (pink). Steady-state measurements were performed at nine potentials from 0.500 to 0.700 V *vs.* Hg/HgO. For each applied potential, the current response was measured for 150 s and the last 25 data points were averaged. All values are 100% *iR* corrected. b) Reaction order plots for NiFe(PBA) LDH (green), NiFe(BA) LDH (blue) and NiFe(BPBA) LDH (pink) at 0.650 V vs. Hg/HgO. For that, five KOH electrolyte solutions with concentrations of 0.2, 0.4, 0.6, 0.8 and 1 M were used. The LSV data was collected at a scan rate of 5 mV s^{-1} using a three-electrode setup with GC as the counter electrode and Hg/HgO as the reference.

in the mechanism can either be an electron transfer step or a chemical reaction. All elementary reactions following the rate determining step do not affect the reaction rate and can be ignored in determining the RDS. Additionally, the calculation assumes the reaction pathway stated by Bockris[9] (Table 1), in which an intermediate adsorbed peroxide is formed. We also made a statement about the symmetry factor β which can deviate from its ideal value of 0.5.[25,40] The reason for that can be the unsymmetrical potential distance profile during an electron exchange step.[25,41]

Therefore, additional mechanistical aspects have to be considered through the electrochemical reaction order, which provides the relationship between the concentration of one reactant species and the reaction rate.[39] The electrochemical reaction order $m_{OH,E}$ is mathematically defined as in Equation (2).

$$m_{OH,E} = \left(\frac{\partial \log i}{\partial \log a_{OH}}\right)_E \quad (2)$$

Here, a_{OH} is the hydroxide ion activity and E is the potential. For the determination of $m_{OH,E}$, reaction order plots for all three candidates were experimentally obtained at 0.650 V *vs.* Hg/HgO. This potential was selected as it represents the midpoint of the high Tafel region (cf. Figure 4). Therefore, activity measurements at five different electrolyte concentrations (0.2 – 1.0 M KOH) were conducted, and the logarithmic current densities at 0.650 V (*vs.* Hg/HgO) were plotted against the respective logarithmic ion activity (OH^-) (Figure 5b). The slopes then represent the occurring reaction order $m_{OH,E}$ at the given potential.

Fractional reaction orders for hydroxide anions have been previously reported.[5,39,42] Here, the fractional values were assumed to be caused by competing reaction pathways and thus the combination of the expected kinetic parameters for the different pathways, so not-rate determining steps or other mechanisms might also influence the reaction order. The fraction of active sites involved in each particular pathway determines the relative contribution of the pathway to the reaction order.[5,42] In such cases, the fractional reaction order can be explained using Temkin adsorption conditions. A detailed derivation of the underlying formulas based on Temkin adsorption conditions can be found in our previous work.[25] Assuming the second step of the Bockris' path as rate determining, the following terms are valid for b and $m_{OH,\eta}$ (Equation (3) and (4)).

$$b = \left(\frac{\partial \eta}{\partial \log f_T}\right)_{a_{OH}} = \frac{2.303\ RT}{F\ (1 + \beta\ -\ \gamma)} \quad (3)$$

$$mOH,\eta = \left(\frac{\partial \ln f_T}{\partial \ln a_{OH}}\right)_\eta = 2 - \gamma \quad (4)$$

Here, NiFe(BA) LDH shows a reaction order of $m_{OH} = 1.37$, suggesting a symmetry factor of $\gamma = 0.63$ and a Tafel slope of $b = 104\ mV\,dec^{-1}$, fitting to a symmetry factor of $\beta = 0.19$. NiFe(PBA) LDH exhibits a reaction order of 1.18, which fits with a symmetry factor of $\gamma = 0.82$. The corresponding Tafel slope of $b = 114\ mV\,dec^{-1}$ can be rationalized with a symmetric potential energy barrier constant of $\beta = 0.33$. Finally, for NiFe(BPBA) LDH a reaction order of 1.26 was obtained, which calculates to $\gamma = 0.74$. It shows a Tafel slope of $b = 131\ mV\,dec^{-1}$, which translates to a symmetry factor of $\beta = 0.18$.

All symmetry factors lay between 0 and 1 when assuming the second step as rate determining, meaning that for all candidates the second adsorption of a hydroxide ion and the formation of the hydrogen peroxide intermediate is rate determining. It also confirms our assumptions about the adsorption conditions and mechanism, as Temkin adsorption and the Bockris path are the only conditions that rationalize the measured Tafel slopes together with the measured reaction orders.

Lastly, stability measurements were made to investigate how the catalysts performance changes due to usage. Therefore, the catalytic activity before and after 24 h electrolysis was investigated by LSV (Figure 6). For both candidates, a slight increase in activity could be observed, which is in good agreement with previous studies, where the activity increase was attributed to the incorporation of residual Fe into the LDH structure.[43] Furthermore, Dionigi *et al.* proved that, under applied anodic potential, NiFe LDH oxidizes from the initial α-phases to activated γ-phases potentially leading to increased activities after aging.[44] Aside from the occurring activation mechanisms, the exchange of the anions with carbonate can rather be excluded, as the activity should decrease when an exchange with carbonate anions occurs.

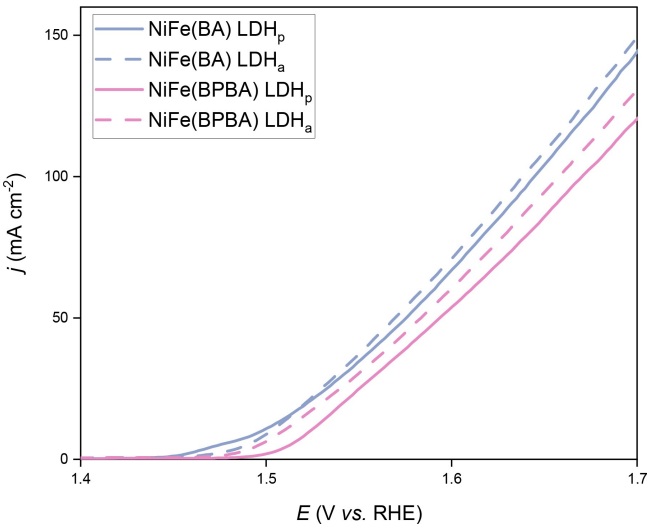

Figure 6. Comparison of OER polarization curves of pristine (p) and aged (a) (dashed lines, 24 h at 1.7 V vs. Hg/HgO) NiFe(BA) LDH (blue) and NiFe(BPBA) LDH (pink). The data points were received at a scan rate of 5 $mV\,s^{-1}$ using a three-electrode setup with glassy carbon as the counter electrode and Hg/HgO as the reference in 1 M KOH as electrolyte.

Conclusions

In this work, we have investigated the underlying mechanisms of alkaline OER on borate intercalated NiFe LDH. We intercalated NiFe LDH with boric acid (BA), tetraborate (TB), phenylborate (PBA), benzene-1,4-diborate (BDBA) and 4-biphenylborate (BPBA) to explore the influence of inorganic and organic borates on the catalysts activity and chose three interesting candidates NiFe(BA) (PBA) and (BPBA) LDH for a kinetic study. All investigated candidates showed dual Tafel behavior and fractional reaction orders, that could be rationalized by the occurrence of Temkin adsorption conditions and the overcoming of the onset potential. We found that the Bockris' path, where a physisorbed hydrogen peroxide intermediate is formed, was prevalent for all three candidates. Here, the second OH^- adsorption step was found to be the rate determining step, which agrees with the findings of our previous work. Furthermore, we found that the intercalation of boric acid into NiFe LDH resulted in excellent catalytic performance in alkaline OER, reflected by a low charge transfer resistance and the lowest Tafel slope at high current densities. Fast kinetics and high conductivity are suggested to be due to the high p*K*a value of borate, which is beneficial for efficient OER catalysis.

Experimental Section

All reactants and solvents are commercially available and of analytical grade and were used without further purification. 4-Biphenylboronic acid (BPBA), benzene-1,4-diboronic acid (BDBA), Nickel(II) nitrate hexahydrate, sodium tetraborate decahydrate (TB) and sodium hydroxide were purchased from Sigma-Aldrich, boronic acid (BA), ethanol abs. and potassium hydroxide from ChemSolute, phenylboronic acid (PBA) from Thermo Scientific and ferric(III) nitrate nonahydrate was bought at Merck. Deionized water was degassed with N_2 for 1 h and used to prepare all reaction solutions.

Herein, NiFe(BA), NiFe(TB), NiFe(PBA), NiFe(BDBA) and NiFe(BPBA) were synthesized *via* a co-precipitation process. For that, 33 mmol $Fe(NO_3)_3 \cdot 6H_2O$ and 66 mmol $Ni(NO_3)_2 \cdot 6H_2O$ were dissolved in 40 mL DI water to form a homogenous solution (solution A, Ni : Fe 2 : 1). Solution B was prepared by dissolving 0.05 mol of the respective anion in 100 mL DI water. In case of NiFe(BDBA) and NiFe(BPBA), the concentration of solution A and B were adjusted to one tenth of the standard concentration due to poor solubility on the anion. The third solution (solution C) was prepared by dissolving 0.34 mol NaOH in 100 mL DI water. For co-precipitation, solution A was added dropwise into solution B, whereas solution C was added to keep the pH value constant at 10. After completely adding solution A, the resulting brown dispersion was stirred for 24 h at room temperature. The precipitate was then filtered under vacuum, washed with DI water until pH 7 and dried at 80 °C. Before preparing catalyst ink, the product was mortared to receive a fine powder.

Electrochemical measurements were performed in a typical three-electrode setup with a glassy carbon counter electrode and a Hg/HgO reference electrode, controlled by a Metrohm Autolab potentiostat PGSTAT302 N. If not mentioned otherwise, 1 M KOH solution in Milliq water was used as the electrolyte. For the working electrode, a polished nickel sheet was used. Before coating the Ni sheet with catalyst ink, the sheet was taped to reduce the area to 1 cm^2. For catalyst ink, 5 mg of catalyst powder was mixed with 900 μL H_2O and 900 μL EtOH sonicated for 30 min to ensure homogeneity. To obtain a uniform loading, 3×10 μL catalyst ink was dropped onto the nickel sheet and dried under a heating lamp, resulting in a catalyst loading of 80 $\mu g\,cm^{-2}$. Lastly, 10 μL of 0.1 % Nafion (Sigma Aldrich) was added for stabilization. For each electrochemical measurement, the electrode was conditioned by running 50 cycles at low scan rates ($\nu = 200\,mV\,s^{-1}$) in order to clean the WE surface.[25,39] The electrocatalytic activity was investigated by CV at a scan rate of $0.005\,V\,s^{-1}$, whereby only the forward scan was considered. For *iR* correction, EIS was measured after each activity test at 0.5 V from 100 kHz to 100 mHz at the amplitude of 10 mV, to obtain the electrolyte resistance. For Tafel plots, steady-state activity measurements were performed at nine potentials in the range of 0.5–0.7 V in 0.025 V steps, whereby every recorded value was given 150 s to reach equilibrium. For *iR* correction of the Tafel values, EIS measurements were conducted at the same potentials. For reaction order plots, CV measurements were performed in different electrolyte concentrations (0.2–1.0 M KOH in 5 steps) at 0.525 V and 0.650 V to cover the Tafel regions.[25] For stability determination, chronoamperometry tests at 1.7 V in a two electrode setup were performed with NiFe(BA) and NiFe(BPBA) for 24 h. Afterwards the electrolyte was carefully exchanged without removing the electrodes and the conditioning and activity testing was done again as described above.

X-ray diffraction (XRD) patterns were measured on a Bruker D2 Phaser device under CuK_α radiation ($\lambda = 1.54$ Å) with 1° incidence angle and 2θ ranging from 6° to 90° with 0.02° steps.

Acknowledgements

This work was funded by the Federal Ministry of Education and Research (H2Giga QT1.5 AlFaKat; FKZ 03HY109B). Open Access funding enabled and organized by Projekt DEAL.

Conflict of Interests

The authors declare no conflict of interest.

Data Availability Statement

The data that support the findings of this study are available at Zenodo: https://doi.org/10.5281/zenodo.13759711

Keywords: Electro kinetic study · Nickel-iron layered double hydroxides · Organic anionic exchange · Oxygen evolution reaction · Water splitting

[1] S. Shiva Kumar, H. Lim, *Energy Rep.* **2022**, *8*, 13793.
[2] A. Karmakar, K. Karthick, S. S. Sankar, S. Kumaravel, R. Madhu, S. Kundu, *J. Mater. Chem. A* **2021**, *9*, 1314.
[3] P. M. Bodhankar, P. B. Sarawade, G. Singh, A. Vinu, D. S. Dhawale, *J. Mater. Chem. A* **2021**, *9*, 3180.
[4] Y. Matsumoto, E. Sato, *Mater. Chem. Phys.* **1986**, *14*, 397.
[5] R. L. Doyle, M. E. G. Lyons, *J. Electrochem. Soc.* **2013**, *160*, H142–H154.
[6] a) S. Anantharaj, K. Karthick, P. Murugan, S. Kundu, *Inorg. Chem.* **2020**, *59*, 730; b) W. Hu, Y. Wang, X. Hu, Y. Zhou, S. Chen, *J. Mater. Chem.* **2012**, *22*, 6010; c) Y. Lee, J. Suntivich, K. J. May, E. E. Perry, Y. Shao-Horn, *J. Phys. Chem. Lett.* **2012**, *3*, 399; d) K. A. Stoerzinger, O. Diaz-Morales, M.

Kolb, R. R. Rao, R. Frydendal, L. Qiao, X. R. Wang, N. B. Halck, J. Rossmeisl, H. A. Hansen, et al., *ACS Energy Lett.* **2017**, *2*, 876.
[7] J. O. Bockris, *J. Chem. Phys.* **1956**, *24*, 817.
[8] R. F. Scarr, *J. Electrochem. Soc.* **1969**, *116*, 1526.
[9] J. O. Bockris, T. Otagawa, *J. Electrochem. Soc.* **1984**, *131*, 290.
[10] S. Trasatti, *J. Electroanal. Chem. Interfacial Electrochem.* **1980**, *111*, 125.
[11] a) J. Rossmeisl, Z.-W. Qu, H. Zhu, G.-J. Kroes, J. K. Nørskov, *J. Electroanal. Chem.* **2007**, *607*, 83; b) I. C. Man, H.-Y. Su, F. Calle-Vallejo, H. A. Hansen, J. I. Martínez, N. G. Inoglu, J. Kitchin, T. F. Jaramillo, J. K. Nørskov, J. Rossmeisl, *ChemCatChem* **2011**, *3*, 1159.
[12] J. Suntivich, K. J. May, H. A. Gasteiger, J. B. Goodenough, Y. Shao-Horn, *Science (New York, N. Y.)* **2011**, *334*, 1383.
[13] S. D. Mürtz, J. Simböck, F. Zeng, M. Ghiasi, S. Schönebaum, U. Simon, F. M. F. de Groot, R. Palkovits, *EES. Catal.* **2023**, *1*, 961.
[14] R. Palkovits, S. Palkovits, *ACS Catal.* **2019**, *9*, 8383.
[15] J. Simböck, M. Ghiasi, S. Schönebaum, U. Simon, F. M. F. de Groot, R. Palkovits, *Nat. Commun.* **2020**, *11*, 652.
[16] a) Z. Sun, L. Lin, J. He, D. Ding, T. Wang, J. Li, M. Li, Y. Liu, Y. Li, M. Yuan, et al., *J. Am. Chem. Soc.* **2022**, *144*, 8204; b) L. Lin, R. Xin, M. Yuan, T. Wang, J. Li, Y. Xu, X. Xu, M. Li, Y. Du, J. Wang, et al., *ACS Catal.* **2023**, *13*, 1431.
[17] Y. Li, M. Yuan, H. Yang, K. Shi, Z. Sun, H. Li, C. Nan, G. Sun, *Appl. Catal. B* **2023**, *323*, 122167.
[18] L. Trotochaud, J. K. Ranney, K. N. Williams, S. W. Boettcher, *J. Am. Chem. Soc.* **2012**, *134*, 17253.
[19] Y. Wang, D. Yan, S. El Hankari, Y. Zou, S. Wang, *Adv. Sci. (Weinheim, Baden-Wurttemberg, Germany)* **2018**, *5*, 1800064.
[20] X. Li, X. Hao, Z. Wang, A. Abudula, G. Guan, *J. Power Sources* **2017**, *347*, 193.
[21] G. Fan, F. Li, D. G. Evans, X. Duan, *Chem. Soc. Rev.* **2014**, *43*, 7040.
[22] M. Luo, Z. Cai, C. Wang, Y. Bi, L. Qian, Y. Hao, L. Li, Y. Kuang, Y. Li, X. Lei, et al., *Nano Res.* **2017**, *10*, 1732.
[23] L. Lv, Z. Yang, K. Chen, C. Wang, Y. Xiong, *Adv. Energy Mater.* **2019**, *9*, 1803358.
[24] D. Zhou, Z. Cai, Y. Bi, W. Tian, M. Luo, Q. Zhang, Q. Xie, J. Wang, Y. Li, Y. Kuang, et al., *Nano Res.* **2018**, *11*, 1358.
[25] M. Berger, I. M. Popa, L. Negahdar, S. Palkovits, B. Kaufmann, M. Pilaski, H. Hoster, R. Palkovits, *ChemElectroChem* **2023**, *10*, e202300235.
[26] K. S. Exner, H. Over, *ACS Catal.* **2019**, *9*, 6755.
[27] L.-F. Li, Y.-F. Li, Z.-P. Liu, *ACS Catal.* **2020**, *10*, 2581.
[28] a) M. Praveen Kumar, M. Sasikumar, A. Arulraj, V. Rajasudha, G. Murugadoss, M. R. Kumar, S. Gouse Peera, R. V. Mangalaraja, *Catalysts* **2022**, *12*, 1470; b) Y. He, S. Zhou, Y. Wang, G. Jiang, F. Jiao, *J. Mater. Sci: Mater. Electron.* **2021**, *32*, 21880.
[29] X. Long, J. Li, S. Xiao, K. Yan, Z. Wang, H. Chen, S. Yang, *Angew. Chem.* **2014**, *126*, 7714.
[30] S. Aisawa, S. Takahashi, W. Ogasawara, Y. Umetsu, E. Narita, *J. Solid State Chem.* **2001**, *162*, 52.
[31] D. G. Evans, R. C. T. Slade *Structure and Bonding* (Eds: X. Duan, D. G. Evans), Springer Berlin Heidelberg, Berlin, Heidelberg **2006**,1–87.
[32] J. L. Anderson, E. M. Eyring, M. P. Whittaker, *J. Phys. Chem.* **1964**, *68*, 1128–1132.
[33] B. M. Hunter, W. Hieringer, J. R. Winkler, H. B. Gray, A. M. Müller, *Energy Environ. Sci.* **2016**, *9*, 1734.
[34] Y. Zhou, S. Xu, Y. Fang, C. Fang, F. Zhu, *J. Clust. Sci.* **2016**, *27*, 1131.
[35] J. A. Carrasco, R. Sanchis-Gual, A. S.-D. Silva, G. Abellán, E. Coronado, *Chem. Mater.* **2019**, *31*, 6798.
[36] a) M. Borkowski, M. Richmann, D. T. Reed, Y. Xiong, *ract* **2010**, *98*, 577; b) M. J. P. A. Batista, M. B. F. Marques, A. S. Franca, L. S. Oliveira, *Foods* **2023**, *12*, 2520.
[37] D. Li, H. Liu, L. Feng, *Energy Fuels* **2020**, *34*, 13491.
[38] A. Karmakar, K. Karthick, S. S. Sankar, S. Kumaravel, R. Madhu, S. Kundu, *J. Mater. Chem. A* **2021**, *9*, 1314.
[39] L. Negahdar, F. Zeng, S. Palkovits, C. Broicher, R. Palkovits, *ChemElectroChem* **2019**, *6*, 5588.
[40] *Photoelectrochemical Solar Fuel Production. From Basic Principles to Advanced Devices* (Eds: J. Bisquert, S. Giménez), Springer International Publishing; Imprint: Springer, Cham **2016**.
[41] R. Guidelli, R. G. Compton, J. M. Feliu, E. Gileadi, J. Lipkowski, W. Schmickler, S. Trasatti, *Pure Appl. Chem.* **2014**, *86*, 245.
[42] A. Carugati, G. Lodi, S. Trasatti, *Mater. Chem.* **1981**, *6*, 255.
[43] a) Z. Qiu, C.-W. Tai, G. A. Niklasson, T. Edvinsson, *Energy Environ. Sci.* **2019**, *12*, 572; b) S. Klaus, Y. Cai, M. W. Louie, L. Trotochaud, A. T. Bell, *J. Phys. Chem. C* **2015**, *119*, 7243; c) L. Trotochaud, S. L. Young, J. K. Ranney, S. W. Boettcher, *J. Am. Chem. Soc.* **2014**, *136*, 6744.
[44] F. Dionigi, Z. Zeng, I. Sinev, T. Merzdorf, S. Deshpande, M. B. Lopez, S. Kunze, I. Zegkinoglou, H. Sarodnik, D. Fan et al., *Nat. Commun.* **2020**, *11*, 2522.
[45] a) C. Hao, R. Zhang, W. Wang, Y. Liang, J. Fu, B. Zou, H. Shi, *J. Solid State Electrochem.* **2019**, *23*, 2343; b) K. Zielinkiewicz, D. Baranowska, E. Mijowska, *RSC Adv.* **2023**, *13*, 16907; c) X. Liu, J. Shi, X. Bai, W. Wu, *Ultrason. Sonochem.* **2021**, *81*, 105840; d) M. E. G. Lyons, R. L. Doyle, M. P. Brandon, *Phys. Chem. Chem. Phy.: PCCP* **2011**, *13*, 21530.

Manuscript received: July 14, 2024
Revised manuscript received: August 23, 2024